Improved modeling of multiple scattering in the Voxel Monte Carlo model

Iwan Kawrakow[a)]
Clinic of Radiation Therapy and Oncology, Radiological Center, University of Leipzig, Liebigstr. 20a, 04103 Leipzig, Germany

(Received 20 February 1996; accepted for publication 30 January 1997)

The implementation of an improved model for multiple scattering into the Voxel Monte Carlo (VMC) algorithm for fast electron dose calculation in radiation therapy is presented. The model takes into account path-length corrections (PLC) and lateral displacement in the individual electron steps. The extraction of the scattering power from the available computed-tomography images is discussed. It is shown that with the improved modeling of multiple electron scattering, the VMC algorithm is comparable in accuracy with PRESTA, the electron transport algorithm of EGS4. The problem of double counting of contributions from atomic electrons to the scattering power is considered and a simple solution is found. © *1997 American Association of Physicists in Medicine.* [S0094-2405(97)02004-X]

Key words: electron beam, dose-calculation, Monte Carlo simulations, Voxel Monte Carlo

I. INTRODUCTION

The Monte Carlo (MC) technique is potentially the most accurate method for the calculation of dose distribution from therapeutic electron beams if radiation source and phantom are accurately modeled and a sufficiently large number of particle histories are simulated.[1–3] Two MC codes are presently in widespread use for radiation transport calculations in medicine: ETRAN, developed by Berger and Seltzer[4] (and its descendants SANDYL,[5] CYLTRAN,[6] ACCEPT,[7] ITS[8]) and EGS4, developed by Nelson *et al.*[9]

A number of studies benchmarking EGS4 and ETRAN with experimental data was carried out. It seems that EGS4 calculations compare favorably to measurements obtained for several electron energies on phantoms containing small inhomogeneities.[10–12] Unfortunately, both models require too long a CPU time to perform a full three-dimensional (3D) dose calculation to be acceptable for clinical purposes. For instance, the EGS4 based code SHAPE, developed by Manfredotti *et al.*,[13] required approximately seven hours of CPU time on a DEC VAX 8600 to compute dose distribution for a 6×6 field of 17 MeV electrons with a statistical uncertainty of 3.5%.

Recently, two new Monte Carlo models for dose calculations in radiation therapy which are by an order of magnitude faster than conventional MC codes were presented.

The Macro Monte Carlo (MMC) model[14,15] uses results derived from EGS4 simulations of electron transport through macroscopic spheres of various radii and consisting of a variety of media. Based on these results, electrons are transported in macroscopic steps through the absorber. In its original version (Ref. 14) the MMC algorithm was restricted to a single sphere radius (0.2 cm) and therefore to a constant transport step size. This was later recognized as one of the major reasons for the algorithm to perform poorly at interfaces to low density material. In the new version of the model (Ref. 15) an adaptive step size algorithm that reduces step sizes in the vicinity of heterogeneities was introduced. One obvious disadvantage is that computational time will increase with increasing complexity of the geometry under consideration. In addition, it was shown in Ref. 16 that EGS4 cannot correctly describe electron transport in small spheres. (Systematical errors present in EGS4 are *a priori* present also in the MMC model because EGS4 is used to pre-calculate the MMC data base.) Finally, it must be mentioned that secondary electrons are treated in a very simple manner in the MMC model.

Contrary to the MMC algorithm, the Voxel Monte Carlo (VMC) model[17,18] is a microscopic MC algorithm using as EGS4 and ETRAN the condensed history method. Introducing some approximations and simplifications into the transport algorithm the computational speed was increased by a factor of 35 compared to EGS4. One of the main disadvantages of the model is the simplified treatment of multiple scattering (by a Gaussian distribution). Also, as in the standard version of EGS4, lateral displacement in the individual electron steps is neglected and path-length corrections are described according to the Fermi–Eyges theory.[19]

The scope of the present paper is to discuss the implementation of the multiple scattering approach of Ref. 20 and the longitudinal and lateral correlation algorithm (LLCA) presented in Ref. 16 into the VMC model. Furthermore, the connection between the mass density and the scattering power of tissues relevant to radiation therapy is studied. A simple solution of the problem of double counting of contributions from atomic electrons to the scattering power, recently discussed by Li and Rogers,[21] is presented. Finally, some test calculations for pencil beams are carried out and the results are compared to EGS4 calculations.

II. MULTIPLE SCATTERING, PATH-LENGTH CORRECTIONS, LATERAL DISPLACEMENT

One of the main difficulties in describing electron transport by the Monte Carlo technique results from the very large number of electron interactions with surrounding matter. Modern Monte Carlo electron transport algorithms (e.g. EGS4,[9] ETRAN,[22] ITS[23]) do not model every electron elastic

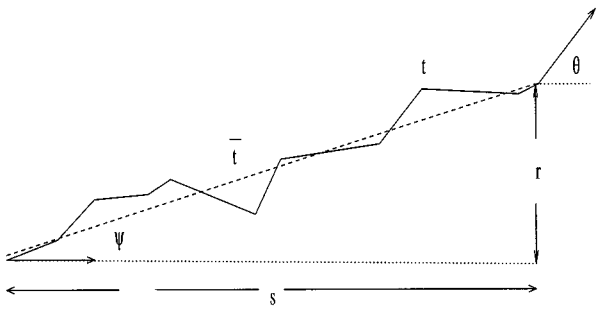

FIG. 1. The curved electron path; θ denotes the multiple scattering angle at the end of the step, ψ the lateral deflection angle which is correlated to θ, $\bar{t}$ is the straight line distance between the initial and final position of the electron, and t is the curved path length.

scattering, but use distributions resulting from many single collisions to describe the change of the direction of the particle motion (condensed history). In this manner a large amount of computational time is saved. Unfortunately, it turns out that for energies below 10 or 20 MeV the results depend strongly on the step size used in the Monte Carlo simulation.[24–26] This step size dependence is mainly due to the difference between the lengths of the electron's curved path and its straight-line path and due to the lateral displacement from the initial direction of motion (see Fig. 1).

In the initial version of the VMC model, discussed in detail in Ref. 18, lateral displacement in the individual electron steps is neglected and PLC is modeled in a simple way according to the Fermi–Eyges theory. In this paper it will be shown in which manner the multiple scattering theory of Ref. 20 and the LLCA-algorithm of Ref. 16 can be implemented into the VMC model without significant loss of computational speed. Before we discuss the approximations required, let us give a brief summary of the multiple scattering theory and the LLCA.

We consider an electron with the total energy (kinetic plus rest energy) E in an infinite unbounded homogeneous phantom initially moving in z direction. The scattering properties of the surrounding matter are described by the quantities b_c and χ_{cc} (for definition see Ref. 20 or 9). The multiple scattering theory of Ref. 20 is formulated in terms of the ''reduced momentum transfer'' y. The connection between the scattering angle θ at the end of a step of the length t and y is given by

$$\cos\,\theta = 1 - \frac{\chi_{cc}^2 t}{2E^2\beta^4} y^2, \tag{1}$$

where β is the electron's velocity (in units of c). According to the results of Ref. 20, the multiple scattering distribution with respect to y reads

$$F(\lambda,y) = \frac{2}{y_0^2}(1-\eta_1-\eta_2)\exp\left(-\frac{y^2}{y_0^2}\right) + \frac{2\mu_1^2\eta_1}{(y^2+\mu_1^2)^2} + \frac{4\mu_2^4\eta_2}{(y^2+\mu_2^2)^3} \tag{2}$$

with parameters $y_0, \mu_1, \mu_2, \eta_1$ and η_2 depending on λ, the average number of elastic collisions during the step under consideration,

$$\lambda = \frac{b_c t}{\beta^2}. \tag{3}$$

Due to the rotational symmetry of the problem the azimuthal angle ϕ is distributed uniformly between 0 and 2π. So, the final direction of motion $\vec{u}$ is given by

$$u_x = \sin\,\theta\,\cos\,\phi, \qquad u_y = \sin\,\theta\,\sin\,\phi, \qquad u_z = \cos\,\theta. \tag{4}$$

We want to note that the simple form of Eq. (2) allows for a very fast sampling of the scattering angle (2–3 times faster than the standard EGS4 multiple scattering subroutine).

According to the LLCA the final position of the electron is given by

$$\begin{aligned} x &= \bar{t}\,\sin\,\psi\,\cos(\phi+\tilde{\phi}),\\ y &= \bar{t}\,\sin\,\psi\,\sin(\phi+\tilde{\phi}),\\ z &= \bar{t}\,\cos\,\psi, \end{aligned} \tag{5}$$

Here, $\tilde{\phi}$ is the angle between the two-dimensional vectors (u_x,u_y) and (x,y) perpendicular to the initial direction of motion, ψ the lateral deflection angle (see Fig. 1), and $\bar{t}$ the average straight line distance between the initial and final electron position. Because the distribution in the angle $\tilde{\phi}$ depends only very slowly on the step size, it is possible to sample $\tilde{\phi}$ from a look-up table pre-calculated by a single scattering Monte Carlo model. (In PRESTA this angle is set to zero. We found it important to sample $\tilde{\phi}$ from the real distribution to improve the step size stability of the LLCA.) For $\bar{t}$ we have

$$\overline{t^2} = \frac{2t^2}{\xi}\left(1 - \frac{1-\exp(-\xi)}{\xi}\right) \tag{6}$$

with the short-hand notation

$$\xi = \tfrac{1}{2} T_s t. \tag{7}$$

The quantity T_s is defined as

$$T_s = \frac{2b_c}{\beta^2}(1-\langle\cos\,\Theta\rangle), \tag{8}$$

where $\langle\cos\Theta\rangle$ is the average scattering angle in a single electron scattering. At high energies T_s is approximately equal to the linear scattering power. The lateral deflection angle ψ is correlated to the scattering angle θ according to

$$\cos\,\psi = 1 - \alpha(1-\cos\,\theta) \tag{9}$$

with

$$\alpha \approx \frac{1}{3}\left(1 + \frac{\xi}{4} + \frac{\xi^2}{360} - \frac{19\xi^3}{4320}\cdots\right). \tag{10}$$

The above formulas are valid for the case where energy loss during the step is neglected. In Ref. 16 a simple approach was found to take energy loss into account:

(1) Use the average electron energy during the step, $E_{1/2}$, to sample the scattering angle;
(2) use $E_{1/2}$ to calculate $\underline{\xi}$;
(3) use $E_{1/2}$ to calculate $t_{1/2}$ and $\alpha_{1/2}$ from Eqs. (6) and (10);
(4) then correct t and α according to

$$\alpha=\alpha_{1/2}(1-\epsilon/4),$$
$$\underline{\underline{t}}=\underline{\underline{t}}_{1/2}\frac{1-\alpha_{1/2}(1-\exp(-\xi))}{1-\alpha_{1/2}(1-\exp(-\xi))(1-\epsilon/4)}, \tag{11}$$

where ϵ is the energy loss fraction during the step under consideration.

This simple approach is also the main reason to introduce a maximum electron step, $t_{\max}$, allowed in order for LLCA to work properly:

$$t_{\max}=\min\left(\frac{1}{T_s},t_{1/2}\right), \tag{12}$$

where $t_{1/2}$ denotes the path length during which the electron loses half of its initial kinetic energy.

III. IMPLEMENTING LLCA INTO VMC

One of the reasons for the improved speed of the VMC model compared to conventional Monte Carlo models such as EGS4 and ETRAN is the new variance reduction technique implemented. The basic idea is as follows: the electron history is generated in an infinite unbounded homogeneous phantom (e.g. water) and then ''applied'' on step-by-step basis several times to different regions of the geometry under consideration. In this section we will discuss in which manner the LLCA and multiple scattering theory can be implemented into the transport algorithm of the VMC.

A. Extracting material properties from the computed-tomography images

Let us denote the mass density, total stopping power, and scattering properties of the medium where the electron history was generated (reference medium) by ρ_0, S_0, and $b_{c,0}, \chi_{cc,0}$. (When delta particle production and bremsstrahlung production are explicitly taken into account in the simulation, then S_0 has to be taken to be the restricted stopping power for the cutoff energies used.) We consider an electron step of the path length t_0 in the reference medium and assume that the step takes place in a medium with the properties ρ, S, b_c, χ_{cc}. To guarantee that the energy loss in this medium is equal to the energy loss in the reference medium we have to rescale the path length by the ratio of the stopping powers, i.e.,

$$t=t_0\frac{S_0}{S}. \tag{13}$$

With this path length the average number of elastic collisions λ in the actual medium will be

$$\lambda=\frac{b_c t}{\beta^2}=\lambda_0\frac{b_c S_0}{b_{c,0}S}=\lambda_0 f_\lambda, \tag{14}$$

where λ_0 denotes the average number of elastic interactions in the reference medium. The ''reduced momentum transfer'' y must then be sampled from the distribution $F(\lambda,y)$ (see the previous section). The scattering angle θ at the step end in the actual medium will be

$$\cos\,\theta=1-\frac{\chi_{cc}^2 t}{2E^2\beta^4}y^2=1-\frac{\chi_{cc}^2 S_0}{\chi_{cc,0}^2 S}(1-\cos\,\theta_0)$$
$$=1-f_\chi(1-\cos\,\theta_0), \tag{15}$$

where θ_0 denotes the scattering angle corresponding to y in the reference medium. We see from Eqs. (14) and (15) that we need two quantities to describe the scattering properties in the medium of interest compared to the reference medium: f_λ and f_χ.

If the chemical composition of the medium under consideration is known, then f_λ and f_χ can be simply calculated. In radiation therapy the geometry is defined via the available computed-tomography (CT) images, so only the Hounsfield numbers of the different voxels are known. One possible approach to circumvent this difficulty is to subdivide the whole Hounsfield range into several intervals, to choose for every interval one typical tissue, and to calculate f_λ and f_χ for this tissue. We use instead another approach: we have calculated f_λ and f_χ for all materials relevant to radiation therapy given in ICRU-Report 46.[27] Water was used as a reference medium. For the ratio S_0/S we have used the fitted curves of Ref. 18 instead of the exact value (the exact ratio is somewhat energy dependent) because these fitted curves are used in practical calculations to extract the stopping powers from the available CT images. In Figs. 2 and 3 f_λ and f_χ as a function of ρ/ρ_0 are shown. The solid lines are fits to the calculated data (circles). Whereas in the case of f_λ the fit

$$f_\lambda=\begin{cases}0.815+0.143\rho/\rho_0, & \rho/\rho_0\geqslant 1.2,\\ 1.0, & 1.034\leqslant\rho/\rho_0<1.2,\\ 0.508+0.406\rho/\rho_0, & 0.918\leqslant\rho/\rho_0<1.034,\\ 0.953, & \rho/\rho_0<0.918\end{cases} \tag{16}$$

describes the data to within 3% of accuracy, in the case of f_χ there are several outliers. The tissues for which f_χ differs to more than 10% from the fit curve

$$f_\chi=\begin{cases}0.916+1.047\,\ln\,\rho/\rho_0, & \rho/\rho_0\geqslant 1.2,\\ 1.107, & 1.138\leqslant\rho/\rho_0<1.2,\\ -0.352+1.282\rho/\rho_0, & 0.92\leqslant\rho/\rho_0<1.138,\\ 0.993-0.18\rho/\rho_0, & \rho/\rho_0<0.92\end{cases} \tag{17}$$

are summarized in Table I.

Here, some remarks are in order. First of all, it has to be noted that the only way to accurately model the scattering properties of the materials from Table I is to manually segment the CT images and then to define by hand the materials involved. This may be a rather lengthy procedure and so not acceptable for routine treatment planning.

On the other hand, the multiple scattering theory we are going to implement into the VMC model is based on Molière's single scattering theory.[28] In Ref. 21 up to 10%

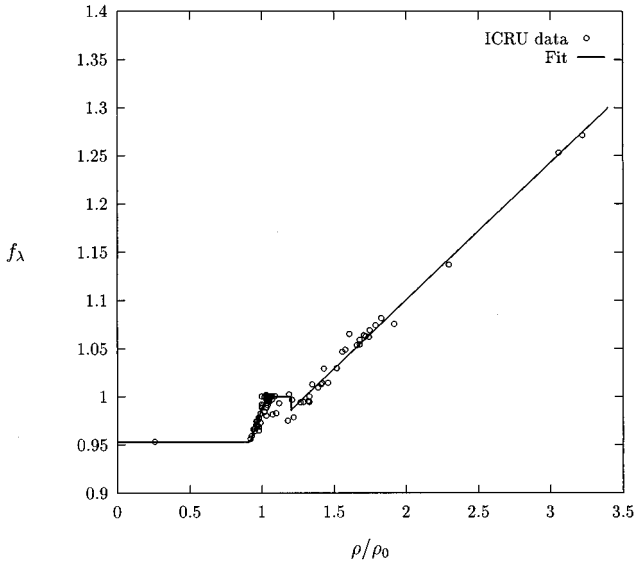

FIG. 2. The quantity f_λ, defined in Eq. (14), for all tissues given in the ICRU Report No. 46 (Ref. 27) as a function of the ratio of the mass density of the medium ρ to the mass density of the reference medium ρ_0. The circles represent f_λ as calculated from the composition of the various materials, the line is the corresponding fit, Eq. (16).

deviations between the linear scattering power resulting from Molière's theory and from the theory of Rossi[29] (used by the ICRU) was found (the linear scattering power is proportional to f_χ). In Ref. 30 single electron scattering within the partial wave method was studied and large deviations to Molière's single scattering theory were observed. We can therefore conclude that the uncertainties resulting from the use of Eq. (17) to extract the scattering properties from the available CT images are of the same order as the uncertainties due to our present knowledge of the scattering properties of materials relevant to radiation therapy. So, the use of Eq. (17) to calculate f_χ may be sufficiently accurate for our purposes.

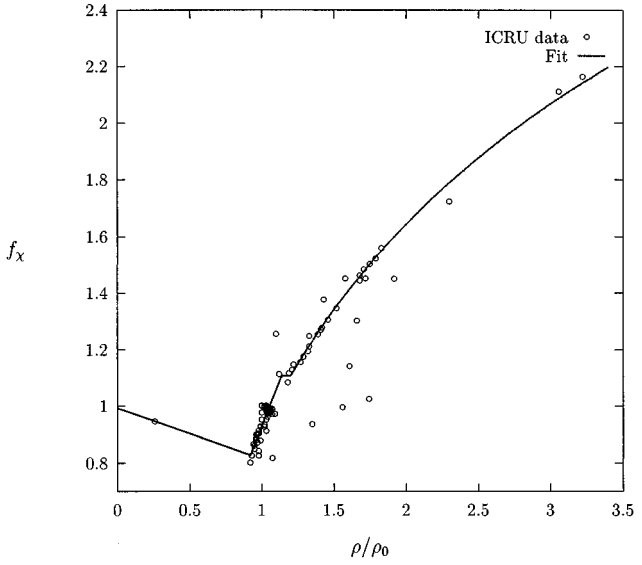

FIG. 3. The quantity f_χ, defined in Eq. (15), for all tissues given in the ICRU Report No. 46 (Ref. 27) as a function of the ratio of the mass density of the medium ρ to the mass density of the reference medium ρ_0. The circles represent f_χ as calculated from the composition of the various materials, the line is the corresponding fit, Eq. (17).

TABLE I. ICRU-tissues for which the exact f_χ value differs by more than 10% to the fit, Eq. (17). (Δf_χ is the relative error in %).

Tissue	ρ(g/cm^3)	Δf_χ (%)
Carbohydrate	0.98	−38.7
Gallstones-cholesterol	1.075	−25.6
Protein	1.35	−31.5
Skeleton-cartilage (Adult)	1.1	15.6
Skeleton-cortical bone (Adult)	1.92	−10.3
Skeleton-cranium (whole) (Adult)	1.61	−24.3
Urinary (renal) stones-cystine	1.66	−11.2
Urinary (renal) stones-uric acid	1.745	−46.3

Finally, to get an estimate of the error resulting from the incorrect modeling of the scattering properties of a medium, we have calculated the depth dose curve for a monoenergetic broad beam of 10 MeV electrons in the ICRU tissue *skeleton-cranium*. For this tissue the fit curve, Eq. (17), overestimates f_χ by approximately 25% (see Table I). In the first calculation the calculated $f_\chi = 1.141$ was used, in the second calculation f_χ was set to 1.415, as resulting from Eq. (17). The results are shown in Fig. 4. The maximum deviation between both curves is 6% of the maximum dose. Note that in practical situations there will be only relatively small regions with this medium and so the error will be even smaller.

B. Approximations

The LLCA briefly discussed in Section II is valid only for electron transport in an infinite unbounded homogeneous phantom. In practical calculations there are heterogeneities

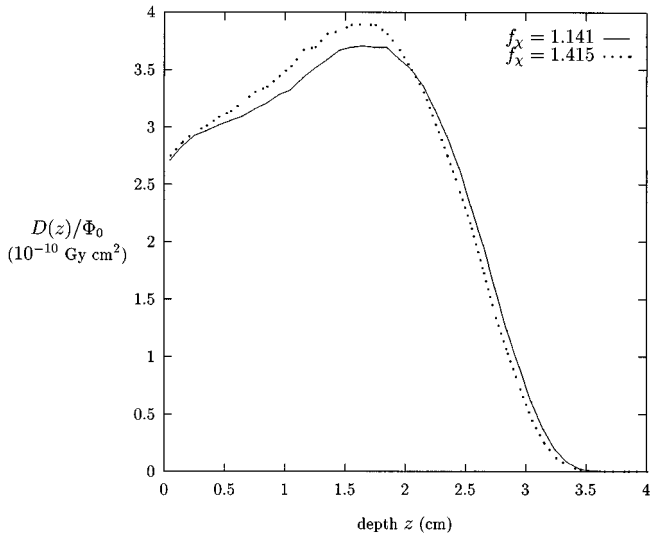

FIG. 4. Depth dose curve calculated in the ICRU-tissue *skeleton-cranium* for 10 MeV monoenergetic electron broad beam. In the first calculation (full line), the exact value of f_χ was used, in the second calculation (dotted line), f_χ was set to the value resulting from the fit, Eq. (17).

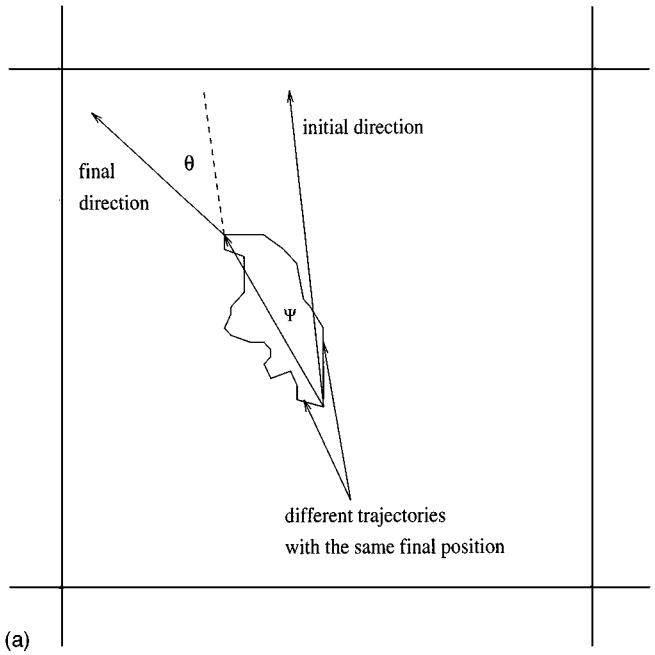

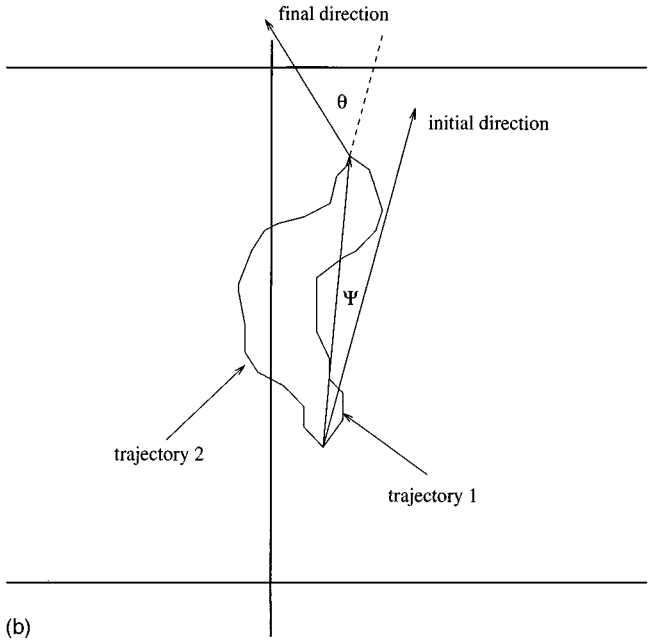

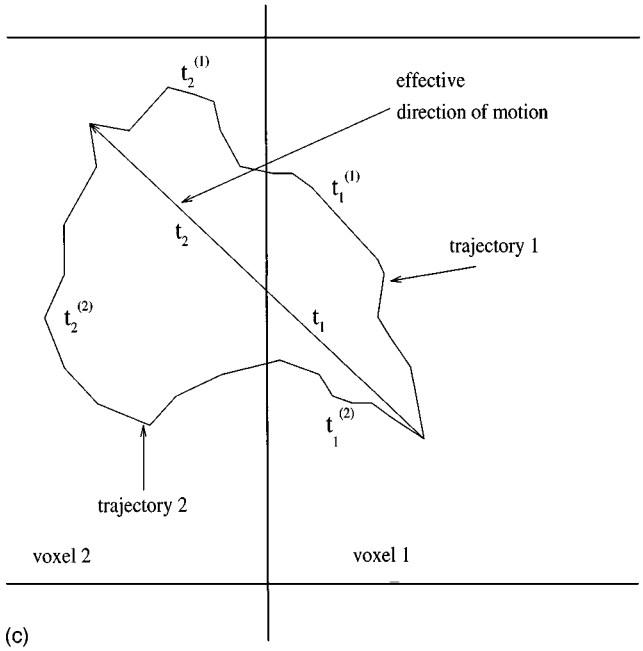

FIG. 5. The problem of boundary crossing; (a) in this case the perpendicular distance of the electron to the nearest boundary is greater than the path length. Therefore, all possible trajectories are in the initial region; (b) the initial and final electron position lie in the same region but portions of the electrons trajectory may be in the neighboring region; (c) the initial and final electron position are in different regions, different possible trajectories correspond to different boundary crossing positions.

and voxel boundaries. To apply the LLCA in this case some approximations must be employed. These approximations will be discussed in this section.

We consider first the situation where the phantom is homogeneous. From our LLCA we have only knowledge about the probability distribution to find an electron at a certain position and moving in a certain direction after traveling a path of the length t. We have no knowledge about the electron's trajectory between the initial and the final position. If the electron is far enough from boundaries (i.e., the perpendicular distance to the nearest boundary is greater than t), then all possible trajectories will be within the present region (see Fig. 5a). So, the electron can be transported between the initial and final position on a straight line. Consider the situation shown in Fig. 5b. Whereas in the case of trajectory 1 the whole energy loss will be deposited in voxel 1, in the case of the trajectory 2 portions of the energy loss will be deposited in voxel 2. When the initial and the final position are in different voxels (Fig. 5c) then we must know which portions of the energy loss have to be deposited in voxel 1 and 2.

An exact solution of the problem of boundary crossing can be achieved only by a single scattering Monte Carlo algorithm, i.e., by a Monte Carlo algorithm where every individual collision is explicitly modeled. If so, the electrons move on straight lines between interaction points and therefore the exact boundary crossing position can be found.

In PRESTA, the transport algorithm of EGS4, the above dif-

ficulties are modeled by reducing the step sizes in the vicinity of boundaries: The maximum step size that can be taken is $t_\perp$, where $t_\perp$ denotes the perpendicular distance to the nearest boundary. If $t_\perp$ becomes smaller than a user defined minimum path length $t_{\min}$, $t_{\min}$ is used and lateral deflection is neglected. This procedure has the advantage of allowing for a very precise modeling of boundary crossing by reducing $t_{\min}$. One obvious disadvantage is, especially if we are interested in a fast dose calculation, that calculation time rapidly increases with decreasing $t_{\min}$.

In the case of VMC, we are going to ''apply'' the history generated in the infinite unbounded reference medium to the geometry of interest. So, it is not possible to implement something like the boundary crossing algorithm of PRESTA. Instead, we introduce the first approximation **A1**:

A1: Transport the electron on a straight line between the initial and final position, as sampled from the LLCA.

It has to be noted that in the situation shown in Fig. 5b the error resulting from the neglect of energy deposition in the neighboring voxel will be, at least partially, compensated by the error from the situation where the electron was in voxel 2 and energy deposition in voxel 1 was neglected. In the case of the electron step shown in Fig. 5c, $t_1/(t_1+t_2)$ and $t_2/(t_1+t_2)$ represent a rather good estimate of the *average* energy loss portions deposited in voxel 1 and 2 from all possible trajectories with the same initial and final position.

There are additional difficulties in the case of heterogeneous phantoms. Let us consider an electron step of length t_0 from a history generated in the reference medium $S_0, b_{c,0}, \chi_{cc,0}$. The continuous energy loss during this step is $\Delta E_0 = S_0 t_0$ and the number of elastic collisions in the reference medium is λ_0. Suppose that this step is passing through several voxels with different materials when ''applied'' to the geometry of interest. Let us denote the path length in the ith voxel by t_i and the properties of the medium in this voxel by S_i and $b_{c,i}, \chi_{cc,i}$ (or $f_{\lambda,i}$ and $f_{\chi,i}$, see the previous subsection). The total number of elastic interactions during this step is (we neglect for simplicity energy loss in the following formulas)

$$\lambda = \sum \frac{b_{c,i} t_i}{\beta^2} = \lambda_0 \sum w_i f_{\lambda,i}, \tag{18}$$

where we have defined

$$w_i = \frac{t_i S_i}{t_0 S_0} = \frac{\Delta E_i}{\Delta E_0}. \tag{19}$$

Here, ΔE_i is the energy deposited in the ith voxel. Remember that the energy loss in the geometry under consideration must be equal to the energy loss in the reference medium and therefore it holds

$$\sum w_i = 1. \tag{20}$$

The multiple scattering angle at the end of the step will be

$$\cos\theta = 1 - y^2 \sum \frac{\chi_{cc,i}^2 t_i}{2E^2\beta^4} = 1 - (1-\cos\theta_0) \sum w_i f_{\chi,i}. \tag{21}$$

In the above equation we have denoted by y the ''reduced momentum transfer'' and by θ_0 the scattering angle in the reference medium corresponding to y. We can conclude from Eqs. (18) and (21) that in order to fix the multiple scattering angle at the end of the step under consideration, we need the path lengths t_i in the different voxels. But these path lengths depend on the effective direction of motion, i.e., direction of motion at the beginning of the step rotated by the lateral deflection angle ψ. The lateral deflection angle ψ is correlated to the scattering angle θ [see Eq. (9)] and thus not known at the beginning of the step. To circumvent this serious problem, we introduce two additional approximations. The first one reads:

A2: Approximate the number of elastic collisions in the geometry under consideration, λ, by the number of elastic collisions in the reference medium, λ_0.

As can be seen from Fig. 2 the maximum error when approximating λ by λ_0 can become about 25% for materials with mass density greater than 3 g/cm^3. In most cases such high density tissues are not involved in the geometry and therefore the error will be smaller than 10%. We show in Fig. 6 a comparison between distributions in the ''reduced momentum transfer'' for λ values differing by 25%. We can conclude from these figures that even when λ was calculated with an error of 25% the resulting effect on the sampled y will be negligible. The approximation **A2** has the additional advantage that the ''reduced momentum transfer'' for a given step y can be sampled from $F(\lambda_0, y)$ during history generation in the reference medium and then used for every history repetition in the geometry of interest.

Let us discuss the next approximation. We have checked that when y is held fixed, the path lengths t_i and therefore the multiple scattering angle and the lateral deflection angle can be determined by the following iterative method:

(1) Calculate the lateral deflection angle ψ using χ_{cc} in the present region;
(2) calculate the effective direction of motion for this ψ;
(3) calculate the path lengths t_i for this effective direction of motion;
(4) recalculate the lateral deflection angle ψ from the multiple scattering angle θ calculated according to Eq. (21) with the actual path lengths t_i;
(5) repeat 2–4 until the change in ψ is smaller than some user defined $\Delta\psi_{\min}$.

This iterative algorithm is demonstrated in Fig. 7 for the situation where the electron is going from a high density region (with large f_χ) to a low density region (with a smaller f_χ). From step 1 we will get a large lateral deflection angle and therefore the direction of motion labeled by ''iteration 1.'' For this direction of motion a large fraction of the electron's step takes place in the lower density region and this leads to a smaller lateral deflection angle and thus to the direction labeled by ''iteration 2.'' The next iteration results

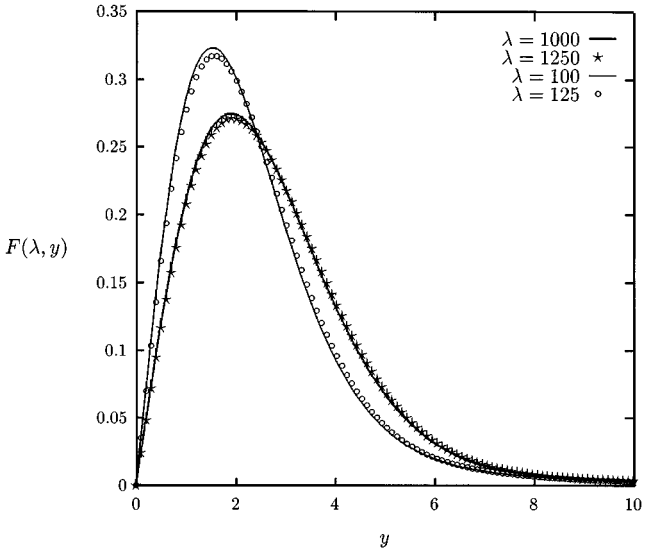

FIG. 6. Comparison between $F(\lambda,y)$ (see the text) for λ values differing by 25%.

in the direction ''3'' and so on. Unfortunately, it turned out that this iterative algorithm (which may be of certain interest for general purpose Monte Carlo models where high precision of boundary crossing is required) is too slow to be implemented in a fast dose calculation algorithm such as VMC. We therefore introduce the last approximation:

A3: Fix the lateral deflection angle for the step under consideration from the scattering properties of the medium in the actual voxel (i.e., perform only step 1 of the above iterative algorithm).

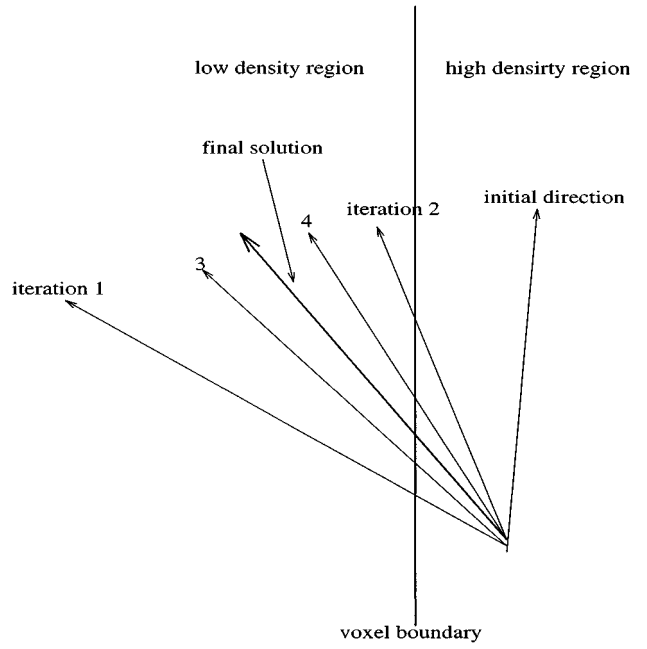

FIG. 7. The iterative algorithm for boundary crossing discussed in Section III B.

This is the most crucial approximation resulting in an overestimate of lateral deflection when going from a high density to a low density medium and vice versa. Note that the multiple scattering angle at the step end is then calculated according to Eq. (21), i.e., the scattering properties of the passed tissues are properly taken into account.

We conclude this subsection with one additional remark concerning the accuracy of the LLCA with the approximations required to implement it into the VMC compared to PRESTA. First of all, it has to be noted that lateral deflection is taken into account, although approximately, in all steps in the transport algorithm discussed above. If we use very short step sizes during history generation in the reference medium (e.g. the minimum transport step size of PRESTA, $t_{\min}$) it will be difficult to prove which algorithm will produce more accurate results in the general case. The examples discussed in Section V seem to indicate that our approach is at least as accurate as PRESTA.

IV. DOUBLE COUNTING OF SCATTERING ON ATOMIC ELECTRONS

In a recent paper by Li and Rogers[21] it was found that scattering on atomic electrons may be double counted in Monte Carlo calculation (depending on the model for multiple scattering):

(1) The contribution of the interactions with atomic electrons to the scattering power is taken into account by replacing Z^2 with $Z(Z+\zeta)$ when calculating the quantities describing the scattering properties of a medium. This is the case in Molière's theory[28,31] and therefore also in EGS4. In EGS4 a default value of $\zeta=1$ is used;
(2) electron-electron collisions with energy transfer greater than a cut off energy E_c (delta particle production) are explicitly taken into account during the simulation according to the Møller cross section.

This double counting may become significant for low Z materials and/or very low values of E_c.

Different methods to take into account the contributions of inelastic collisions to the scattering power were discussed for instance in Ref. 32 (see also references therein). A recent approach was presented in Ref. 33.

Before we start with the discussion of the solution we are going to propose, it has to be noted that the replacement $Z^2\rightarrow Z(Z+\zeta)$ is only an approximation (see for instance the article by Scott[34]). It is therefore not *a priori* clear whether after removing double counting we will obtain more accurate results. If we for instance assume that $Z^2\rightarrow Z(Z+\zeta)$ underestimates the contribution from electrons, then $Z^2\rightarrow Z(Z+\zeta)$ together with inelastic Møller interactions may produce more accurate results. So, the main advantage from correction of double counting proposed here will be that the results will become independent on the cut off energy for Møller collisions used.

We consider for simplicity atomic materials. In this subsection we will denote the scattering angle in a single elastic collision by Θ and the multiple scattering angle by θ. The

multiple scattering theory we are going to implement in the VMC model is based on the screened Rutherford cross section to describe single elastic scattering

$$\frac{d\sigma_R}{d\ \cos\ \Theta}=\frac{2\pi r_e^2 Z(Z+\zeta)}{\beta^2\tau(\tau+2)}\frac{1}{(1-\cos\Theta+\chi_a^2/2)^2}, \tag{22}$$

where χ_a denotes the screening angle and r_e, Z, τ, and β are the electron classical radius, atomic number, ratio of kinetic energy of the electron to its rest energy, and velocity of the electron relative to the velocity of light in vacuum, respectively. Now we define, in analogy to the mass scattering power,[35] the quantity T_R/ρ,

$$\frac{T_R(\zeta)}{\rho}=\frac{1}{\rho}\frac{d\langle\sin^2\ \theta\rangle_R}{ds}\bigg|_{s\to 0}, \tag{23}$$

where $\langle\cdots\rangle_R$ means averaging of $\sin^2\theta$ with the multiple scattering distribution $f_R(\theta)$ resulting from collisions described by the scattering law σ_R given in Eq. (22). Because $\langle\sin^2\theta\rangle=\langle\theta^2\rangle+\langle O(\theta^4)\rangle$, the quantity T_R/ρ behaves very similarly to the linear mass scattering power. The use of $\langle\sin^2\theta\rangle$ instead of $\langle\theta^2\rangle$ allows one to perform the following calculations analytically. According to the theory of Goudsmit and Saunderson,[36] which is applicable for all scattering angles and path lengths, $f_R(\theta)$ after traveling a path length s (for very thin foils the path length can be taken to be equal to the foil thickness s) reads

$$f_R(\theta)=\frac{1}{2}\sum_{l=0}^{\infty}(2l+1)P_l(\cos\ \theta)e^{-Q_l}, \tag{24}$$

where P_l are Legendre polynomials and

$$Q_l=N\int_0^s ds'\int_0^\pi d\cos\ \Theta[1-P_l(\cos\ \Theta)]\frac{d\sigma_R}{d\ \cos\ \Theta}. \tag{25}$$

Here, N denotes the density of scattering centers. Combining Eqs. (22)–(25) and using the properties of the Legendre polynomials we get

$$\frac{T_R(\zeta)}{\rho}=\frac{4\pi N_A r_e^2}{\beta^2\tau(\tau+2)}\frac{Z(Z+\zeta)}{A}g_R(\chi_a) \tag{26}$$

with $N_A=6.022045\times 10^{23}$ Avogadro's constant, A the relative atomic mass, and $g_R(\chi_a)$ defined via

$$g_R(\chi_a)=\left(1+\frac{\chi_a^2}{2}\right)\ln\left(1+\frac{4}{\chi_a^2}\right)-2. \tag{27}$$

In analogy to T_R/ρ we define now the quantity T_M/ρ,

$$\frac{T_M}{\rho}=\frac{1}{\rho}\frac{d\langle\sin^2\ \theta\rangle_M}{ds}\bigg|_{s\to 0}, \tag{28}$$

where $\langle\cdots\rangle_M$ means averaging of $\sin^2\theta$ with the multiple scattering distribution $f_M(\theta)$ resulting from inelastic collisions described by the Møller differential cross section[37] σ_M,

$$\frac{d\sigma_M}{d\tau'}=\frac{2\pi r_e^2}{\beta^2}\frac{1}{\tau'^2}\left[1+\frac{\tau'^2}{(\tau-\tau')^2}+\frac{\tau'^2}{(\tau+1)^2}-\frac{2\tau+1}{(\tau+1)^2}\frac{\tau'}{\tau-\tau'}\right], \tag{29}$$

where τ' denotes the ratio of the kinetic energy of the secondary electron to its rest energy. Note that by definition the secondary electron is the electron with the lower energy, i.e., $\tau'\leqslant\tau/2$. The scattering angle resulting from the production of a delta particle with τ' is

$$\sin^2\ \theta(\tau,\tau')=\frac{2\tau'}{\tau(\tau-\tau'+2)}. \tag{30}$$

Due to the fact that Møller collisions are associated with energy loss it is not possible to derive an expression for f_M corresponding to Eq. (24). But for very thin foils where the average number of Møller interactions is much smaller than unity, f_M can be approximated by the single scattering law σ_M, and we can write

$$\frac{T_M(\tau_c)}{\rho}=\frac{4\pi N_A r_e^2}{\beta^2\tau(\tau+2)}\frac{Z}{A}g_M(\tau,\tau_c), \tag{31}$$

where τ_c is the ratio of the cutoff kinetic energy for delta particle production to the electron's rest energy and the function $g_M(\tau,\tau_c)$ is given by

$$\begin{aligned}g_M(\tau,\tau_c)&=\int_{\tau_c}^{\tau/2}d\tau'\ \sin^2\ \theta(\tau,\tau')\frac{d\sigma_M}{d\tau'}\\&=\ln\frac{\tau}{2\tau_c}+\left[1+\frac{(\tau+2)^2}{(\tau+1)^2}\right]\ln\frac{2(\tau-\tau_c+2)}{\tau+4}\\&\quad-\left[\frac{(\tau+2)^2}{4}+\frac{(\tau+2)(\tau+1/2)}{(\tau+1)^2}\right]\\&\quad\times\ln\frac{(\tau+4)(\tau-\tau_c)}{\tau(\tau-\tau_c+2)}\\&\quad+\frac{(\tau-2\tau_c)(\tau+2)}{2}\left[\frac{1}{\tau-\tau_c}-\frac{1}{(\tau+1)^2}\right].\end{aligned} \tag{32}$$

When τ is below the threshold for delta particle production, $2\tau_c$, then $g_M(\tau,\tau_c)$ must be set to zero.

We now assume that for $\zeta=\zeta_0$, $T_R(\zeta_0)$ correctly describes the total contribution from atomic electrons to the scattering power. To guarantee that there is no double counting of collisions with atomic electrons when Møller interactions with energy transfer greater than τ_c are explicitly modeled in the Monte Carlo calculation, we must use $\zeta=\zeta_M$ with

$$\frac{T_R(\zeta_0)}{\rho}=\frac{T_R(\zeta_M)}{\rho}+\frac{T_M(\tau_c)}{\rho} \tag{33}$$

to calculate the quantities describing the scattering properties of the medium (i.e., χ_{cc}). From Eqs. (26), (31), and the definition of χ_{cc},

$$\chi_{cc}^2(\zeta)=4\pi N_A r_e^2 m^2\rho\frac{Z(Z+\zeta)}{A} \tag{34}$$

(m is the mass of the electron in MeV), we obtain

$$\chi^2_{cc}(\zeta_M)=\chi^2_{cc}(\zeta_0)\left[1-\frac{1}{Z+\zeta_0}\frac{g_M(\tau,\tau_c)}{g_R(\chi_a)}\right]. \tag{35}$$

In other words, when performing a Monte Carlo simulation of electron transport with a cut off energy for delta particle production τ_c we must calculate $\chi_{cc}(\zeta_M)$ for every electron step in dependence on τ_c, τ, and the screening angle χ_a, and then use this $\chi_{cc}(\zeta_M)$ to sample the multiple scattering angle.

In the case of polyatomic substances χ_{cc} is given by

$$\chi^2_{cc}(\zeta)=4\pi N_A r_e^2 m^2 \rho \frac{\Sigma Z_i(Z_i+\zeta)}{\Sigma p_i A_i}, \tag{36}$$

where p_i is the relative weight of the ith element and the sum runs over all elements of the mixture. The only change that is required for Eq. (35) is to replace the factor $1/(Z+\zeta_0)$ by $1/\overline{Z}$,

$$\frac{1}{\overline{Z}}=\frac{\Sigma p_i Z_i}{\Sigma p_i Z_i(Z_i+\zeta_0)}. \tag{37}$$

It has to be noted that the total scattering power resulting from collisions with atomic electrons alone, T_e/ρ, can be calculated from

$$\frac{T_e}{\rho}=\frac{T_R(\zeta_0)}{\rho}-\frac{T_R(0)}{\rho}. \tag{38}$$

For a given electron energy and a given screening angle, T_e/ρ is a constant, whereas T_M/ρ increases with decreasing τ_c. It is therefore clear that for some critical cutoff energy T_{cc}, T_M/ρ will become equal to T_e/ρ, i.e., the total scattering power due to electrons is taken into account only by inelastic Møller interactions. For cutoff energies even smaller than the critical, the scattering power due to electrons will be overestimated. Fortunately, it turns out that T_{cc} is of the same order as the effective ionization energy. The Møller cross section is derived neglecting binding effects (i.e., considering both electrons as free). Therefore, only calculations with cutoff energy for delta particle production much larger than the ionization energy of the medium of interest are meaningful. So, there will be no problems with the approach presented here.

To test the reliability of our approach, we have simulated electron transport in an infinite, unbounded, homogeneous water phantom with different cutoff energies and calculated the average squared scattering angle $\overline{\theta^2}$ after a given path length t. In Fig. 8 the ratio $R=\overline{\theta^2}/\overline{\theta_0^2}$ is shown, where $\overline{\theta_0^2}$ denotes the average squared scattering angle in the calculation where Møller scattering was switched off. To demonstrate the effect of double counting, the results of the calculations without the correction described in this section are also shown in the figure.

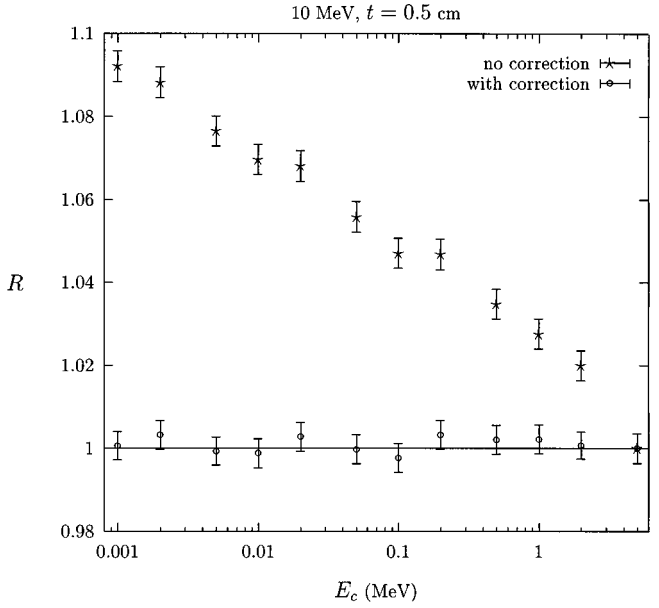

FIG. 8. The ratio R of $\overline{\theta^2}$, the average squared scattering angle after a given path length t calculated with inelastic Møller interactions taken into account, to $\overline{\theta_0^2}$, the average squared scattering angle after the same path length calculated with Møller scattering switched off, as a function of the cutoff energy for Møller collisions, E_c. To demonstrate the effect of double counting, $\overline{\theta^2}/\overline{\theta_0^2}$ calculated without the correction proposed in this paper is also shown.

V. EXAMPLES

In the original VMC paper, good agreement between VMC and EGS4 calculations was found in a variety of geometries for broad beams. In this paper we will study dose distribution for pencil beams because this distribution is much more sensitive to the correct modeling of multiple scattering. The EGS4 calculations were carried out with default PRESTA parameters for two different total cutoff energies for Møller scattering: 521 keV and 700 keV ($ECUT$ was always set equal to AE). Although relative easy to implement in EGS4, the correction discussed in the last section was not used. To estimate the resulting error we have calculated the depth dose curves of a pencil electron beam of 5 MeV kinetic energy using $\zeta_0=1$ and $\zeta_0=0$ (i.e., setting the parameter FUDGEMS to 1 and 0 in PEGS4). For $\zeta_0=1$ the contribution of atomic electrons to the scattering power is overestimated and for $\zeta_0=0$ underestimated. The results are shown in Fig. 9. For comparison the depth dose curve calculated with $AE=700$ keV is also shown. We see from this figure that the error due to double counting of collisions with atomic electrons is smaller than the deviation between the calculations with $AE=700$ keV and $AE=521$ keV. So, in the remaining calculations discussed in this section in all cases $\zeta_0=1$ was used for EGS4. The deviation between the calculations with different cutoff energies for Møller scattering can be explained as follows: As mentioned in the previous section, PRESTA uses step sizes equal to $t_{\min}$ in the vicinity of boundaries and lateral deflection is neglected. With the default PRESTA parameters, $t_{\min}$ is fixed from the cutoff energy for Møller scattering and is 0.0032 cm for $AE=521$ keV or 0.044 cm for $AE=700$ keV in water respectively. The smaller $t_{\min}$ is, the smaller is the number of steps where the lateral deflection is neglected. In addition, a lower value of

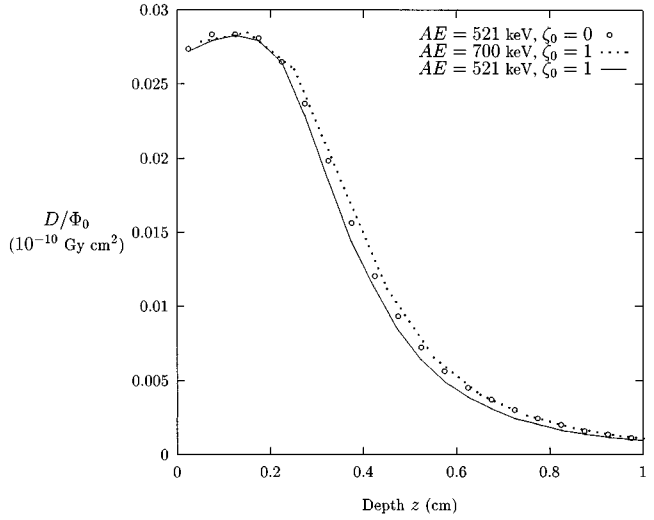

FIG. 9. The effect of double counting of scattering with atomic electrons on the dose distribution of a 5 MeV pencil beam; All curves were calculated with EGS4 and default PRESTA parameters. The difference between the calculation with $AE=521$ keV, $\zeta_0=1$ and $AE=521$ keV, $\zeta_0=0$ is smaller than the difference between $AE=521$ keV, $\zeta_0=1$ and $AE=700$ keV, $\zeta_0=1$. For an explanation see the text.

$t_{\min}$ causes in the presence of boundaries shorter electron steps and therefore a smaller error due to the neglect of lateral displacement. Thus, it can be expected that the calculation with $AE=521$ keV is more accurate than the calculation with $AE=700$ keV when the default PRESTA parameters are used.

All VMC calculations were performed with a cutoff kinetic energy $E_c=0.2$ MeV for Møller scattering. The user parameter $ESTEPE$ (analogous to $ESTEPE$ in EGS4) was set to 0.05.

In Fig. 10 the depth dose curve for a 5 MeV pencil beam in water is shown. The line represents EGS4 with $AE=521$ keV, the stars EGS4 with $AE=700$ keV, and the circles VMC results. We see an excellent agreement between the VMC and EGS4 ($AE=521$ keV) calculations. In Fig. 11 dose profiles at depth of 0.25 cm (11a) and 0.95 cm (11b) as calculated with VMC (circles) and EGS4 ($AE=521$ keV) are depicted. The agreement is again very good.

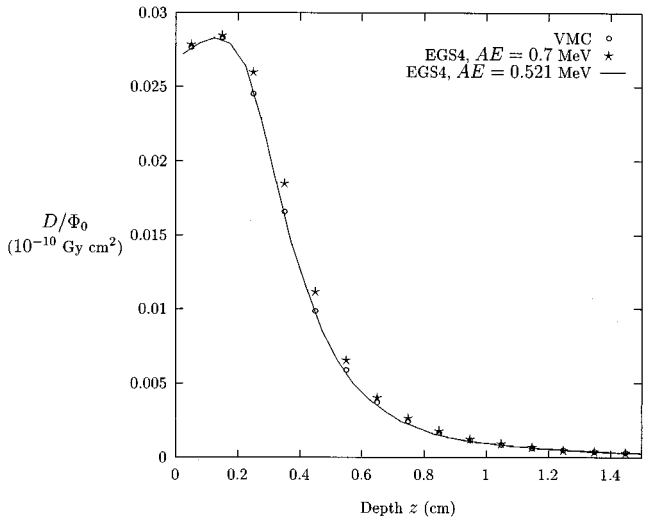

FIG. 10. Comparison between the depth dose curves in a water phantom calculated with VMC (circles) and EGS4. The EGS4 calculations were carried out with default PRESTA parameters and $AE=521$ keV (line) and $AE=700$ keV (stars). The initial energy of the pencil beams was 5 MeV.

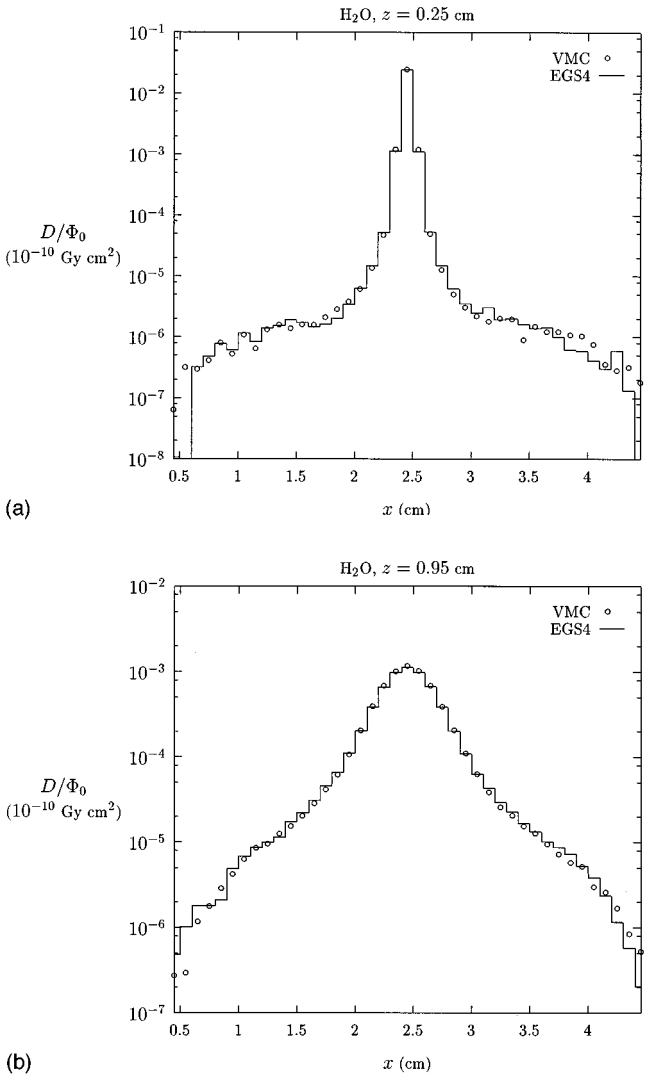

FIG. 11. Comparison between dose profiles calculated with VMC and EGS4 for the same conditions as in Fig. 10; Only the EGS4 results for $AE=521$ keV (lines) are shown. (a) Dose profile at a depth of 0.25 cm; (b) dose profile at a depth of 0.95 cm.

As a next example, the dose distribution for a 5 MeV pencil beam in aluminum was calculated. (Aluminum can be considered as the upper limit of tissues relevant to radiation therapy.) The different depth dose curves are shown in Fig. 12. The symbols have the same meaning as in Fig. 10. Here, we observe deviations between VMC and EGS4 with $AE=521$ keV. These deviations are however smaller than the deviations between both EGS4 calculations with different cut off energies. Note that in addition to the approximations **A1–A3** discussed in Section III B, the collision and radiation stopping powers in aluminum are also treated in an approxi-

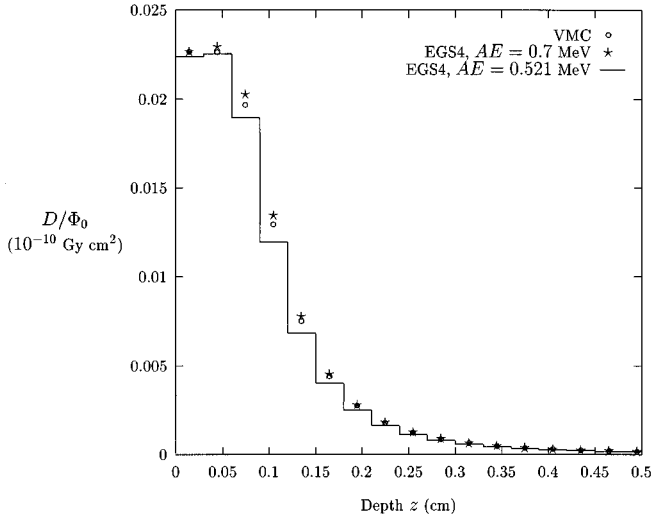

FIG. 12. The same as in Fig. 10 but in a homogeneous aluminum phantom.

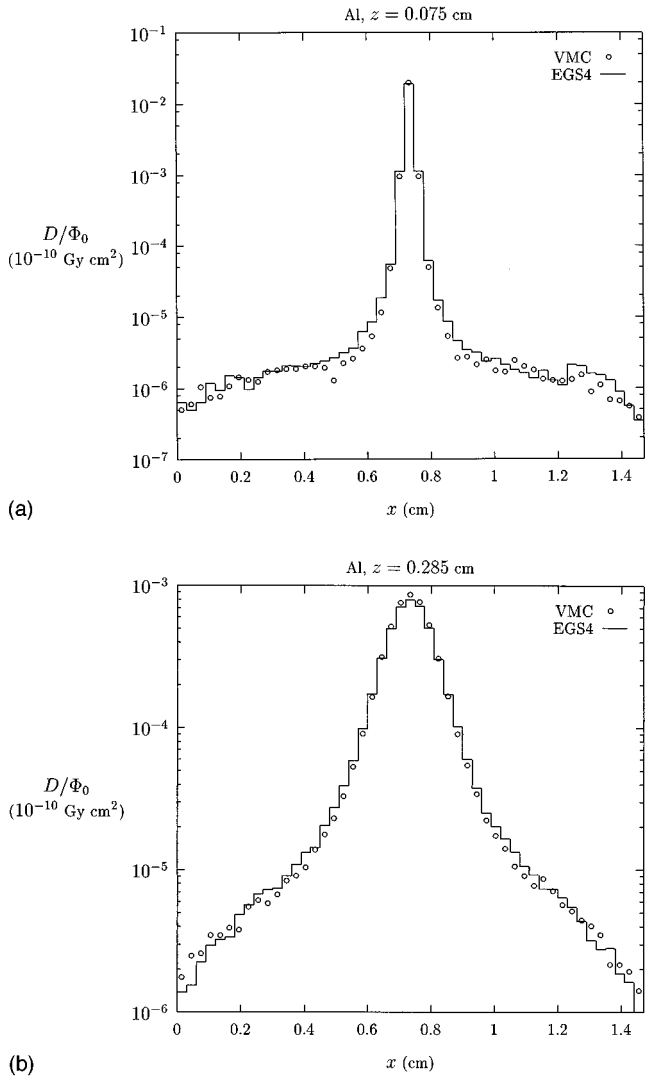

FIG. 13. Comparison between dose profiles calculated with VMC and EGS4 for the same conditions as in Fig. 12; only the EGS4 results for $AE = 521$ keV (lines) are shown. (a) Dose profile at a depth of 0.075 cm; (b) dose profile at a depth of 0.285 cm.

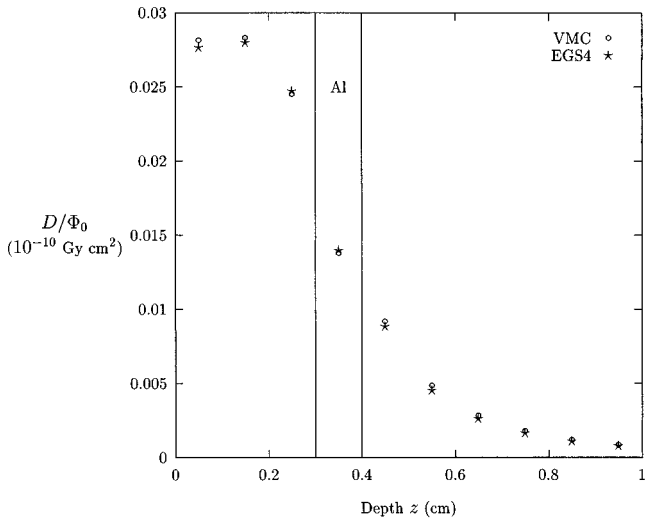

FIG. 14. Depth dose curves calculated with VMC (circles) and EGS4 (stars) for a 5 MeV pencil beam incident on a water phantom with an aluminum inhomogeneity described in the text. The EGS4 calculation was performed with $AE = 521$ keV.

mate manner in the VMC calculation [see Eqs. (19) and (20) in the original VMC paper, Ref. 18]. It is remarkable to see that all these approximations have a smaller net effect on the dose distribution than the minimum step size used in the EGS4 calculation! In Fig. 13 dose profiles for two different depths are depicted. It can be seen from this figure that the slight dose overprediction on the central axis in the VMC calculation is compensated by a slight dose underprediction in the neighboring voxels, whereas the dose distribution at large distances from the central axis is rather well reproduced.

To test the accuracy of the VMC model in heterogeneous geometries we consider as a next example dose distribution for a 5 MeV pencil beam in a water phantom with an aluminum inhomogeneity, 1 mm thick, having a lateral extension of 3×3 mm^2, centered at the beam axis at a depth of 3 to 4 mm. In Fig. 14 the depth dose curve for this geometry calculated with VMC (circles) and EGS4 ($AE = 521$ keV) is depicted. Figure 15 shows dose profiles at depths of 3.5 mm (going through the inhomogeneity) and 4.5 mm (0.5 mm behind the inhomogeneity). We see in all cases an excellent agreement between VMC and EGS4.

We can conclude from the examples considered in this section that with the new multiple scattering theory and LLCA implemented, the VMC model performs dose calculations in tissues relevant to radiation therapy with an accuracy comparable to the accuracy of EGS4. We have shown in this paper only results for 5 MeV electrons. For other energies, the calculated dose distributions show similar features as the dose distributions discussed above.

Compared to the initial version of the VMC model[18], the CPU time required for a dose calculation increased by approximately 25%. Nevertheless, implemented on a low cost 133 MHz Pentium©-PC, the improved model performs 3D dose calculation for a 10×10 field of 20 MeV electrons and

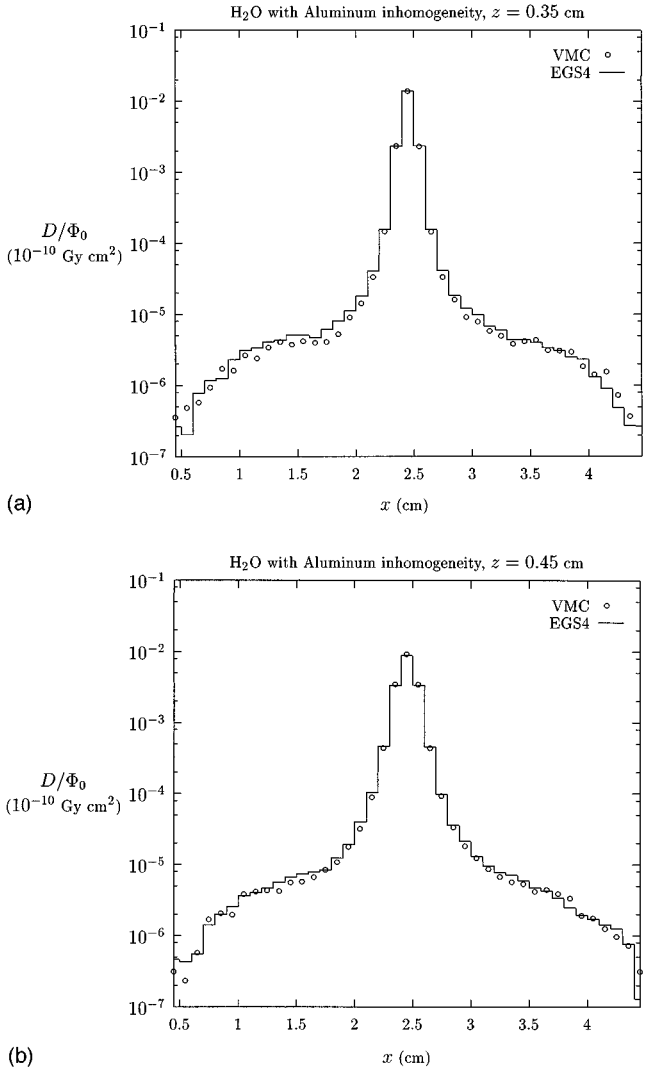

FIG. 15. Comparison between dose profiles calculated with VMC and EGS4 for the same conditions as in Fig. 14; (a) dose profile at a depth of 0.35 cm (the plane of the inhomogeneity); (b) dose profile at a depth of 0.45 cm (0.5 mm behind the inhomogeneity).

$0.5\times0.5\times0.5$ cm^3 voxel sizes within seven minutes of CPU time. Thus, we consider the improved VMC model to be applicable for routine treatment planning.

VI. SUMMARY

In this paper the implementation of the new multiple scattering theory presented in Ref. 20 and the new Lateral-Longitudinal-Correlation-Algorithm (LLCA) from Ref. 16 into the VMC model was discussed. LLCA takes into account both the difference between the curved electron path and the straight line distance to the final position (known as path-length correction), and the deflection of the electron from its initial direction of motion in a single step (known as lateral displacement). It was shown in which manner the scattering properties of the materials involved in the geometry under consideration can be extracted from the available CT images. The approximations necessary to implement LLCA into the VMC model were explained in detail. The example calculations considered in Section V seem to indicate that the improved VMC model is comparable in accuracy with EGS4. Although the CPU time required for a 3D dose calculation increased compared to the initial version of the model[18] by approximately 25%, VMC is fast enough to be applicable in routine treatment planning.

In Section IV the problem of double counting of contributions of atomic electrons to the scattering power that may occur in Monte Carlo calculations was addressed. The proposed method to solve this problem, initially mentioned in a paper by Li and Rogers,[21] was shown to remove the dependence of the mean scattering angle on the cutoff energy for inelastic Møller interactions. This method, now implemented in the VMC model, can be easily employed into the EGS4 too.

ACKNOWLEDGMENTS

The presented work was supported by the Deutsche Forschungsgemeinschaft (DFG) under contract No. FR 941/1-3. The author is grateful to Dr. A. F. Bielajew of the National Research Council of Canda and to Dr. M. Fippel of the University of Leipzig for reading this manuscript prior submission.

[a]Present address: Ionizing Radiation Standards, National Research Council of Canada, Ottawa, K1A 0R6, Canada.

[1]D. Rogers and A. Bielajew, ''Monte Carlo techniques of electron and photon transport for radiation dosimetry,'' in *The Dosimetry of Ionizing Radiation*, edited by K. Kase, B. Bjärngard and F. Attix (Academic, New York, 1990).

[2]T. Mackie, ''Applications of the Monte Carlo method in radiotherapy,'' in Ref. 1.

[3]P. Andreo, ''Monte Carlo techniques in medical radiation physics,'' Phys. Med. Biol. **36**, 861–920 (1991).

[4]M. J. Berger and S. M. Seltzer, ''Tables of Energy-Deposition Distributions in Water Phantoms Irradiated by Point-Monodirectional Electron Beams with Energies from 1 to 60 MeV, and Applications to Broad Beams,'' Natl. Bur. Stand. (U.S.) Report No. NBSIR-82-2451, 1982.

[5]H. M. Colbert, ''SANDYL: A computer program for calculating combined photon-electron transport in complex systems,'' Sandia Laboratories, Livermore, Report Number SCL-DR-720109, 1973.

[6]J. A. Halbleib and W. H. Vandevender, ''CYLTRAN,'' Nucl. Sci. Eng. **61**, 288 (1976).

[7]J. A. Halbleib, Sandia Laboratories Report No. SAND-79-0415, 1979.

[8]J. A. Halbleib and T. A. Mehlhorn, '' ITS: The Integrated TIGER Series of Coupled Electron/Photon Monte Carlo Transport Codes,'' Sandia Laboratories Report No. SAND-84-0573, 1984.

[9]W. R. Nelson, H. Hirayama, and D. W. O. Rogers, ''The EGS4 Code System,'' SLAC Report No. SLAC-265, 1985.

[10]D. W. O. Rogers and A. F. Bielajew, ''Differences in electron depth-dose curves calculated with EGS and ETRAN and improved energy-range relationships,'' Med. Phys. **13**, 687–694 (1986).

[11]K. R. Shortt, C. K. Ross, A. F. Bielajew, and D. W. O. Rogers, ''Electron beam dose distributions near standard inhomogeneities,'' Phys. Med. Biol. **31**, 235–249 (1986).

[12]T. R. Mackie, P. J. Reckwerdt, C. M. Wells, J. N. Yang, J. O. Deasy, M. Podgorsak, M. A. Holmes, D. W. O. Rogers, G. X. Ding, B. A. Faddegon, C. Ma, A. F. Bielajew, and J. Cygler, '' The OMEGA Project: Comparison among EGS4 electron beam simulations, 3-D Fermi-Eyges calculations, and dose measurements,'' *Proceedings of the XIth Conference on the Use of Computers in Radiotherapy* (Medical Physics, Madison, WI), 152–153 (1994).

[13]C. Manfredotti, U. Nastasi, R. Marchisio, C. Ongaro, G. Gervino, R. Ragona, S. Anglesio, and G. Sannazzari, ''Monte Carlo simulation of dose distribution in electron beam radiotherapy treatment planning,'' Nucl. Instrum. Methods A **291**, 646–654 (1990).

[14]H. Neuenschwander and E. Born, ''A macro Monte Carlo method for electron beam dose calculations,'' Phys. Med. Biol. **37**, 107–125 (1992).
[15]H. Neuenschwander, T. Mackie, and P. Reckwerdt, ''MMC—a high-performance Monte Carlo code for electron beam treatment planning,'' Phys. Med. Biol. **40**, 543–574 (1995).
[16]I. Kawrakow, ''Electron transport: longitudinal and lateral correlation algorithm,'' Nucl. Instrum. Methods B **114**, 307–326.
[17]I. Kawrakow, M. Fippel, and K. Friedrich, ''3D Elektronendosisberechnung mit einem voxelorientiertem Monte-Carlo-Algorithmus,'' Medizinische Physik, Proceedings 1994 (unpublished), pp. 180–184.
[18]I. Kawrakow, M. Fippel, and K. Friedrich, ''3D Electron Dose Calculation using a Voxel based Monte Carlo Algorithm,'' Med. Phys. **23**, 445–457 (1996).
[19]H. Messel and D. Crawford, *Electron-Photon Shower Distribution Function* (Pergamon, Oxford, 1970).
[20]I. Kawrakow, ''Electron transport: Multiple and plural scattering,'' Nucl. Instrum. Methods B **108**, 23–34 (1996).
[21]X. Li and D. W. O. Rogers, ''Electron mass scattering powers: Monte Carlo and analytical calculations,'' Med. Phys. **22**, 791–798 (1995).
[22]S. Seltzer, ''An Overview of ETRAN Monte Carlo Methods,'' in *Monte Carlo Transport of Electrons and Photons*, edited by W. Nelson, T. Jenkins, A. Rindi, A. Nahum, and D. Rogers (Plenum, New York, 1989), pp. 153–182.
[23]J. Halbleib, R. Kensek, T. Melhorn, G. Valdez, S. Seltzer, and M. Berger, ''ITS Version 3.0: The Integrated TIGER Series of Coupled Electron/Photon Monte Carlo Transport Codes,'' Sandia Report No. SAND91-1634 (1992).
[24]S. Seltzer and M. Berger, Nucl. Instrum. Meth. **119**, 157 (1974).
[25]D. W. O. Rogers, ''Low energy electron transport with EGS,'' Nucl. Instrum. Methods **227**, 535–548 (1984).
[26]A. F. Bielajew and D. W. O. Rogers, ''PRESTA: The Parameter Reduced Electron-step Transport Algorithm for electron Monte Carlo transport,'' Nucl. Instrum. Methods B **18**, 165–181 (1987).
[27]''Photon, Electron, Proton and Neutron Interaction Data for Body Tissues,'' ICRU-Report No. 46, International Comission on Radiation Units and Measurements, 1992.
[28]G. Molière, ''Theorie der Streuung schneller geladener Teilchen. 1. Einzelstreuung am abgeschirmten Coulomb-Feld,'' Z. Naturforsch. **2a**, 133–145 (1947).
[29]B. Rossi, *High Energy Particles* (Prentice–Hall, New York, 1952).
[30]A. Bielajew, R. Wang, and S. Duane, ''Incorporation of single elastic scattering in the EGS4 Monte Carlo code system: Tests of Molière theory,'' Nucl. Instrum. Methods B **82**, 503–512 (1993).
[31]G. Molière, ''Theorie der Streuung schneller geladener Teilchen. 2. Mehrfach- und Vielfachstreuung,'' Z. Naturforsch. **3a**, 78–97 (1948).
[32]M. J. Berger and R. Wang, '' Multiple-scattering angular deflections and energy-loss straggling,'' in *Monte Carlo Transport of Electrons and Photons*, edited by T. M. Jenkins, W. R. Nelson, A. Rindi, A. E. Nahum, and D. W. O. Rogers (Plenum, New York, 1989), pp. 21–56.
[33]J. Baro, J. Sempau, F. Salvat, and J. Fernandez-Varea, ''PENELOPE: An algorithm for Monte Carlo simulation of the penetration and energy loss of electrons and positrons in matter,'' Nucl. Instrum. Methods B **100**, 31–46 (1995).
[34]W. Scott, ''The theory of small-angle multiple scattering of fast charged particles,'' Rev. Mod. Phys. **35**, 231–313 (1963).
[35]''Radiation dosimetry: Electrons with initial energies between 1 and 50 MeV,'' ICRU-Report No. 21, International Comission on Radiation Units and Measurements, 1972.
[36]S. Goudsmit and J. Saunderson, ''Multiple scattering of electrons,'' Phys. Rev. **57**, 24–29 (1940).
[37]C. Møller, ''Passage of Hard Beta Rays Trough Matter,'' Ann. Phys. **14**, 531 (1932).